*Journal of Sound and Vibration* (2002) **258**(1), 123–146
doi:10.1006/jsvi.5103, available online at http://www.idealibrary.com on IDEAL®

# PRACTICAL ASPECTS IN MOVING LOAD IDENTIFICATION

X. Q. Zhu and S. S. Law

*Civil and Structural Engineering Department, Hong Kong Polytechnic University, Hung Hom, Hong Kong, People's Republic of China. E-mail: cesslaw@polyu.edu.hk*

(*Received* 12 *October* 2001, *and in final form* 27 *February* 2002)

Several methods have been developed in recent years to identify moving loads on top of a continuous beam using measured vibration responses. The methods can identify the forces with some accuracy, but they have not been tested under field measurement conditions with a bridge–vehicle system. This paper discusses the weaknesses and merits of two methods when applied to a single-span bridge deck. The influence, on the moving load identification, of practical aspects such as measurement noise, sampling frequency, a small number of measured response modes, a small number of measuring points, road surface roughness and non-uniform velocity or braking of vehicle is studied in simulations and experiment. Results show that finite element approach with orthogonal function approximation of the responses give more accurate results, in general, than the exact solution approach for all the studies presented in this paper. The road surface roughness and a large variation in the speed are identified as the two main obstacles leading to erroneous results.



## 1. INTRODUCTION

Information of vehicular load on a bridge deck is essential to bridge design as it constitutes the live load component in the bridge design code. Traditionally, the vehicular load was either measured directly from an instrumented vehicle [1, 2] or computed from models of the bridge deck and the vehicle [3–5]. It would be very expensive and the results obtained are subjected to bias in the first approach, while the second approach is subjected to modelling errors. Systems have been developed for weigh-in-motion of the vehicles [6, 7], but they all measured only the static axle loads. A technique to estimate the vehicular loads from the vibration responses of the bridge deck is required such that the different parameters of the bridge and vehicle system are accounted for in the measured responses, and the cost involved would be much less than that by direct measurement.

In the last few years, several methods have been presented by the authors on moving force identification. These methods can be categorized into two groups. One group is based on the exact solution and system identification theory, such as the time domain method (TDM, [8]) and the frequency-time domain method (FTDM, [9]). The bridge deck is modelled as a simply supported beam with viscous damping, and the vehicle/bridge interaction force is modelled as one-point or two-point loads with fixed spacing, moving at constant speed. The correlation of the measured and reconstructed responses is a robust scoring function for evaluating the identified results.

The results obtained from the above methods are noise sensitive and they exhibit large fluctuations at the beginning and at the end of the time histories. These moments correspond to the switching of free vibration state of the structure to the forced vibration state, and *vice versa*, and the solutions are ill conditioned. Law *et al.* [10] introduced a

0022-460X/02/$35.00 

regularization method in the ill-conditioned problem to provide bounds to the identified forces in this group of methods. The results obtained are greatly improved over those without regularization with acceptable errors from using different combinations of measured responses. However, it is difficult to use these methods to identify vehicular loads with multiple axles or vehicles on multi-span continuous bridge due to the long computational time and large computer capacity. Most of the computational time is spent on the computation of the time-varying system matrices. Therefore, another TDM based on regularization technique is developed [11] which gives exact solutions to the forces with improved formulation over existing methods for a more efficient computation.

Another group of methods is based on finite element formulation, such as the interpretive method ITM-I, [12] ITM-II, [13], and the optimal state estimation approach [14]. ITM-I reconstructs the dynamic wheel loads from the bridge strains. The bridge deck is modelled as an assembly of lumped masses interconnected by massless elastic beam elements, not necessarily of the same length. The measured or total responses are caused by the inertial or D'Alembert's forces and the damping forces. ITM-II uses Euler's equation for beams to model the bridge deck in the interpretation of dynamic loads crossing the deck. The optimal state estimation approach uses the dynamic programming technique to provide bounds to the identified forces in solving the ill-conditioned problem in the time domain using different combinations of measured responses in both simulation and laboratory studies. The computational time of ITM [15] is not long compared with TDM and FTDM, but the identification accuracy is much lower. Large errors in the identified results are induced by the direct derivation of the bridge modal responses in the ITM. A general method based on the finite element formulation was later developed [16] in which, a generalized orthogonal function approximation is proposed to obtain the derivatives of the bridge modal responses. The moving loads are identified using least-squares method with regularization in the time domain.

All the above methods are able to identify moving forces with some accuracy. But the effectiveness and accuracy of these methods have not been studied and compared particularly on aspects related to application with field measurement, such as measurement noise, sampling frequency, a small number of sensors, small number of measured response modes, road surface roughness and non-uniform velocity or braking of vehicle. Their performances need to be quantified before their application to real problems. Methods from the two groups [11, 16] are studied with numerical examples and by laboratory work in this paper. Results obtained indicate that the finite element method is in general, better than the exact solution method in the types of problem studied. The road surface roughness and a large variation in the speed are identified as the two main obstacles leading to erroneous results.

## 2. DYNAMIC BEHAVIOUR OF STRUCTURE

The bridge–vehicle system is modelled as a continuous beam subject to a system of moving forces $P_l(t)$ $(l = 1, 2, \ldots N_p)$ as shown in Figure 1. The forces are assumed to be moving as a group at a prescribed velocity $v(t)$, along the axial direction of the beam from left to right. The beam is assumed to be an Euler–Bernoulli beam. The equation of motion can be written as

$$\rho A \frac{\partial^2 w(x,t)}{\partial t^2} + C \frac{\partial w(x,t)}{\partial t} + EI \frac{\partial^4 w(x,t)}{\partial x^4} = \sum_{l=1}^{N_p} P_l(t)\delta(x - \hat{x}_l(t)), \tag{1}$$

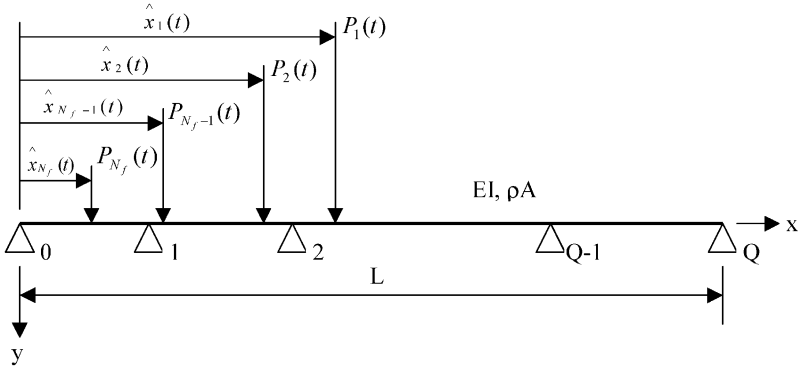


Figure 1. A continuous beam subject to moving loads.

where $L$ is the total length of the beam, $A$ is the cross-sectional area, $E$ is Young's modulus, $I$ is the moment of inertia of the beam cross-section, $\rho$, $C$ and $w(x,t)$ are the mass per unit length, the damping and the displacement function of the beam, respectively, $\hat{x}_l(t)$ is the location of moving force $P_l(t)$ at time $t$, $\delta(t)$ is the Dirac delta function and $N_p$ is the number of forces. The transverse displacement $w(x,t)$ in modal co-ordinates is expressed as

$$w(x,t) = \sum_{i=1}^{\infty} \phi_i(x) q_i(t), \tag{2}$$

where $\phi_i(x)$ is the mode shape function of the $i$th mode, which is determined from the eigenvalue and eigenfunction analysis proposed by Hayashikawa and Watanabe [17]; $q_i(t)$ is the $i$th modal amplitude. Substituting equation (2) into equation (1), and multiplying by $\phi_i(x)$, integrating with respect to $x$ between 0 and $L$, and applying the orthogonality conditions, we obtain

$$\frac{\mathrm{d}^2 q_i(t)}{\mathrm{d}t^2} + 2\xi_i\omega_i \frac{\mathrm{d}q_i(t)}{\mathrm{d}t} + \omega_i^2 q_i(t) = \frac{1}{M_i} \sum_{l=1}^{N_p} P_l(t)\phi_i(\hat{x}_l(t)), \tag{3}$$

where $\omega_i, \xi_i, M_i$ are, respectively, the modal frequency, the damping ratio and the modal mass of the $i$th mode, and

$$M_i = \int_0^L \rho A \phi_i^2(x)\, \mathrm{d}x. \tag{4}$$

The displacement of the beam at point $x$ and at time $t$ can be found from equations (2) and (3):

$$w(x,t) = \sum_{i=1}^{\infty} \frac{\phi_i(x)}{M_i} \int_0^t h_i(t-\tau) \sum_{l=1}^{N_p} P_l(\tau)\phi_i(\hat{x}_l(\tau))\, \mathrm{d}\tau, \tag{5}$$

where

$$h_i(t) = \frac{1}{\omega_i'} \mathrm{e}^{-\xi_i\omega_i t} \sin \omega_i' t, \qquad \omega_i' = \omega_i \sqrt{1-\xi_i^2}. \tag{6}$$

## 3. MOVING FORCE IDENTIFICATION

The two moving load identification methods are briefly described below to provide more background information to engineers to get familiar with the subsequent studies. Dynamic strain measurements will be used in the moving forces identification.

### 3.1. BASED ON EXACT SOLUTION METHOD (ESM) [11]

The strain in the beam at point $x$ and at time $t$ can be written as

$$\varepsilon(x,t) = -z_t \frac{\partial^2 w(x,t)}{\partial x^2}, \tag{7}$$

where $z_t$ is the distance between the under surface and the neutral surface of the beam.

Substituting equation (5) into equation (7), and by rewriting in the discrete form one obtains

$$\varepsilon(x_s,m) = -\sum_{i=1}^{N} \frac{z_t \phi_i''(x_s) \Delta t}{M_i} \sum_{j=0}^{m} h_i(m-j) \sum_{l=1}^{N_p} P_l(j) \phi_i(\hat{x}_l(j))$$
$$(m = 0,1,2,\ldots,N_t, s = 1,2,\ldots,N_s), \tag{8}$$

where $\Delta t$ is the time interval, $N$ is the number of vibration modes, $N_t$ is the number of data points, $x_s$ is the location of the measuring point, $N_s$ is the number of measuring points

$$h_i(j) = \frac{1}{\omega_i'} \mathrm{e}^{-\xi_i \omega_i j \Delta t} \sin \omega_i' j \Delta t. \tag{9}$$

Equation (8) can be rewritten in the matrix form as

$$\mathbf{BP} = \boldsymbol{\varepsilon}, \tag{10}$$

where $\boldsymbol{\varepsilon}$ is $(N_t * N_s) \times 1$ matrix, $\mathbf{B}$ is $(N_t * N_s) \times (N_t * N_p)$ matrix, $\mathbf{P}$ is $(N_t * N_p) \times 1$ matrix,

$$\boldsymbol{\varepsilon} = \{\varepsilon(x_1,1), \varepsilon(x_2,1), \ldots \varepsilon(x_{N_s},1), \varepsilon(x_1,2), \ldots \varepsilon(x_{N_s},N_t)\}^{\mathrm{T}},$$
$$\mathbf{P} = \{p_1(0), p_2(0), \ldots, p_{N_p}(0), p_1(1), \ldots, p_{N_p}(N_t-1)\}^{\mathrm{T}}. \tag{11}$$

When the measured data are more than the number of unknown forces, equation (10) can be solved using the least-squares method. However, the solution would involve the computation of the inverse of matrix $\mathbf{B}$ which would be very inefficient when the measured data is large [8, 9]. Matrix $\mathbf{B}$ can be split into smaller submatrices to improve the computation efficiency as follows:

$$\mathbf{B} = \begin{bmatrix} \mathbf{B}_{10} & 0 & \cdots & 0 \\ \mathbf{B}_{20} & \mathbf{B}_{21} & \cdots & 0 \\ \vdots & \vdots & \vdots & \vdots \\ \mathbf{B}_{N_t 0} & \mathbf{B}_{N_t 1} & \cdots & \mathbf{B}_{N_t N_t - 1} \end{bmatrix}_{(N_s * N_t) \times (N_p * N_t)}, \qquad \mathbf{B}_{mj} = \begin{bmatrix} b_{11} & b_{12} & \cdots & b_{1N_p} \\ b_{21} & b_{22} & \cdots & b_{2N_p} \\ \cdots & \cdots & \vdots & \cdots \\ b_{N_s 1} & b_{N_s 2} & \cdots & b_{N_s N_p} \end{bmatrix}_{N_s \times N_p},$$

$$b_{sl} = z_t \Delta t \sum_{i=1}^{N} \frac{\phi_i''(x_s)}{M_i} h_i(m-j) \phi_i(\hat{x}_l(j))$$
$$(m = 1,2,3,\ldots,N_t, j = 0,1,2,\ldots,N_t - 1, s = 1,2,\ldots,N_s, l = 1,2,\ldots,N_p). \tag{12}$$

### 3.2. BASED ON FINITE ELEMENT FORMULATION (FEM) [16]

The same assumptions of forces moving on top of a continuous beam as discussed above are studied. Substitute equation (2) into equation (7) and assuming there are $N$ modes in the responses, we have

$$\varepsilon(x,t) = \boldsymbol{\varphi}\mathbf{Q}, \tag{13}$$

where

$$\boldsymbol{\varphi} = -\{z_t\phi_1''(x), z_t\phi_2''(x), \cdots, z_t\phi_N''(x)\}, \qquad \mathbf{Q} = \{q_1(t), q_2(t), \ldots, q_N(t)\}^{\mathrm{T}}.$$

and $\phi_i''(x)$ is the second derivative of $\phi_i(x)$.

The strain can be approximated by a generalized orthogonal function $T(t)$ as

$$\varepsilon(x,t) = \sum_{i=1}^{N_f} T_i(t)C_i(x), \tag{14}$$

where $\{T_i(t), i = 1,2,\ldots,N_f\}$ is the generalized orthogonal function [16] and $\{C_i(x), i = 1,2,\ldots,N_f\}$ is the vector of coefficients in the expansion expression. The strains at the $N_s$ measuring points can be expressed as

$$\boldsymbol{\varepsilon} = \mathbf{C} * \mathbf{T} \tag{15}$$

where

$$T = \{T_0(t), T_1(t), \cdots, T_{N_f}(t)\}^{\mathrm{T}},$$
$$\boldsymbol{\varepsilon} = \{\varepsilon(x_1,t), \varepsilon(x_2,t), \cdots, \varepsilon(x_{N_s},t)\}^{\mathrm{T}},$$
$$C = \begin{bmatrix} C_{10}(x_1) & C_{11}(x_1) & \cdots & C_{1N_f}(x_1) \\ C_{20}(x_2) & C_{21}(x_2) & \cdots & C_{2N_f}(x_2) \\ \vdots & \vdots & \vdots & \vdots \\ C_{N_s0}(x_{N_s}) & C_{N_s1}(x_{N_s}) & \cdots & C_{N_sN_f}(x_{N_s}) \end{bmatrix}$$

and $\{x_1, x_2, \ldots, x_{N_s}\}$ is the vector of the location of the strain measurements. By the least-squares method, the coefficient matrix can be obtained as

$$\mathbf{C} = \boldsymbol{\varepsilon} * \mathbf{T}^{\mathrm{T}} * (\mathbf{T} * \mathbf{T}^{\mathrm{T}})^{-1}. \tag{16}$$

Substitute equation (13) into equation (15),

$$\mathbf{Q} = (\boldsymbol{\Phi}^{\mathrm{T}} * \boldsymbol{\Phi})^{-1} * \boldsymbol{\Phi}^{\mathrm{T}} * \mathbf{C} * \mathbf{T}, \tag{17}$$

where

$$\boldsymbol{\Phi} = -\begin{bmatrix} z_t\phi_1''(x_1) & z_t\phi_2''(x_1) & \cdots & z_t\phi_N''(x_1) \\ z_t\phi_1''(x_2) & z_t\phi_2''(x_2) & \cdots & z_t\phi_N''(x_2) \\ \vdots & \vdots & \vdots & \vdots \\ z_t\phi_1''(x_{N_s}) & z_t\phi_2''(x_{N_s}) & \cdots & z_t\phi_N''(x_{N_s}) \end{bmatrix}$$

and it can be obtained from Zhu and Law [16].

The vector of generalized co-ordinates obtained from equation (17) can be substituted into equation (3), and rewritten in matrix form to become

$$\mathbf{I} * \ddot{\mathbf{Q}} + \mathbf{C}_d * \dot{\mathbf{Q}} + \mathbf{K} * \mathbf{Q} = B * P \tag{18}$$

or

$$\mathbf{U} = \mathbf{B} * \mathbf{P}, \tag{19}$$

where

$$\mathbf{C}_d = \text{diag}(2 * \xi_i * \omega_i),$$
$$\mathbf{K} = \text{diag}(\omega_i^2),$$

$$\mathbf{B} = \begin{bmatrix} \phi_1(\hat{x}_1(t))/M_1 & \phi_1(\hat{x}_2(t))/M_1 & \cdots & \phi_1(\hat{x}_{N_p}(t))/M_1 \\ \phi_2(\hat{x}_1(t))/M_2 & \phi_2(\hat{x}_2(t))/M_2 & \cdots & \phi_2(\hat{x}_{N_p}(t))/M_2 \\ \vdots & \vdots & \vdots & \vdots \\ \phi_N(\hat{x}_1(t))/M_N & \phi_N(\hat{x}_2(t))/M_N & \cdots & \phi_N(\hat{x}_{N_p}(t))/M_N \end{bmatrix}.$$

The required $\ddot{\mathbf{Q}}$ and $\dot{\mathbf{Q}}$ can be obtained by directly differentiating equation (17) to obtain

$$\ddot{\mathbf{Q}} = (\mathbf{\Phi}^{\mathrm{T}} * \mathbf{\Phi})^{-1} * \mathbf{\Phi}^{\mathrm{T}} * \mathbf{C} * \ddot{\mathbf{T}},$$
$$\dot{\mathbf{Q}} = (\mathbf{\Phi}^{\mathrm{T}} * \mathbf{\Phi})^{-1} * \mathbf{\Phi}^{\mathrm{T}} * \mathbf{C} * \dot{\mathbf{T}}.$$

It is seen from the formulation of the method that when the modal parameters of the structure are replaced by those from a finite element model, this method could be applied to complex real structure of varying geometry and mass distribution and with different boundary conditions.

### 3.3. REGULARIZATION

The moving forces obtained from equations (10) and (19) using a straightforward least-squares solution would be unbound. A regularization technique can be used to solve the ill-posed problem in the form of minimizing the function

$$J(\mathbf{P}, \lambda) = ||\mathbf{B} * \mathbf{P} - \boldsymbol{\varepsilon}||^2 + \lambda ||\mathbf{P}||^2 \quad \text{or} \quad J(\mathbf{P}, \lambda) = ||\mathbf{B} * \mathbf{P} - U||^2 + \lambda ||\mathbf{P}||^2, \tag{20}$$

where $\lambda$ is the non-negative regularization parameter. The generalized cross validation [18] and L-curve method [19] can be employed to determine the optimal regularization parameter.

## 4. SIMULATION STUDIES

Two examples are used to compare the weaknesses and merits of these methods.

### 4.1. EXAMPLE 1: IDENTIFICATION OF TWO MOVING LOADS ON A SINGLE-SPAN BEAM

A single-span simply supported beam with two forces $p_1(t)$ and $p_2(t)$ moving on top is studied

$$p_1(t) = 20000[1 + 0{\cdot}1 \sin(10\pi t) + 0{\cdot}05 \sin(40\pi t)] \text{ N},$$
$$p_2(t) = 20000[1 - 0{\cdot}01 \sin(10\pi t) + 0{\cdot}05 \sin(50\pi t)] \text{ N}. \tag{21}$$

The parameters of the beam are: $EI = 2{\cdot}5 \times 10^{10}\ \text{N m}^2$, $\rho A = 5000\ \text{kg/m}$, $L = 30\ \text{m}$. The distance between the two moving forces is 4.27 m. The first six natural frequencies of the beam are 3·90, 15·61, 35·13, 62·45, 97·58 and 140·51 Hz. White noise is added to the

calculated responses of the beam to simulate the polluted measurements with

$$\varepsilon = \varepsilon_{calculated} + E_P * N_{oise} * \sigma(\varepsilon_{calculated}), \tag{22}$$

where $\varepsilon$ and $\varepsilon_{calculated}$ are the polluted and the original strains respectively. $E_p$ is the noise level. $N_{oise}$ is a standard normal distribution vector with zero mean value and unit standard deviation and $\sigma(\varepsilon_{calculated})$ is the standard deviation of the original strains.

The errors in the identified forces are calculated as

$$Error = \frac{||P_{identified} - P_{True}||}{||P_{True}||} \times 100\%. \tag{23}$$

The first six modes are used in the simulation. The time interval between adjacent data points is 0·002 s. Six measuring points are evenly distributed on the beam at $1/7L$ spacing. The moving speed is 30 m/s, and 20 terms are used in the orthogonal function. These parameters are used in the following studies unless specified otherwise.

### 4.2. STUDY 1: EFFECT OF NOISE LEVEL

Monte Carlo method is used to simulate the noise in the responses, and noise levels are from 1 to 10%. Figure 2 shows the mean and standard deviation of the errors in the identified moving loads using the method based on ESM, and Figure 3 shows those from using the method based on FEM.

The errors from using ESM vary approximately linearly with the noise levels in the responses. The standard deviation in the errors is largest with 6% noise in the responses.

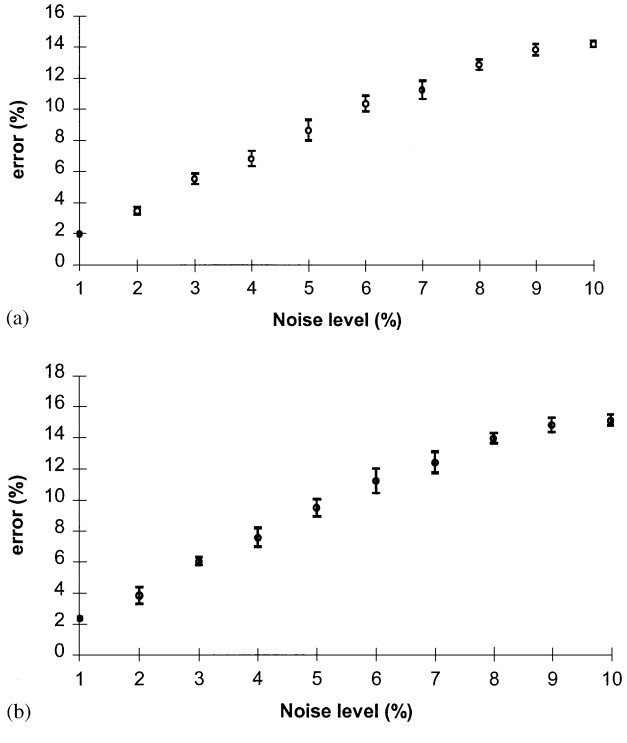


Figure 2. The mean (circles) and standard deviation (error bars) of the errors in the identified moving loads using ESM: (a) errors in the identified first moving load and (b) errors in the identified second moving load.

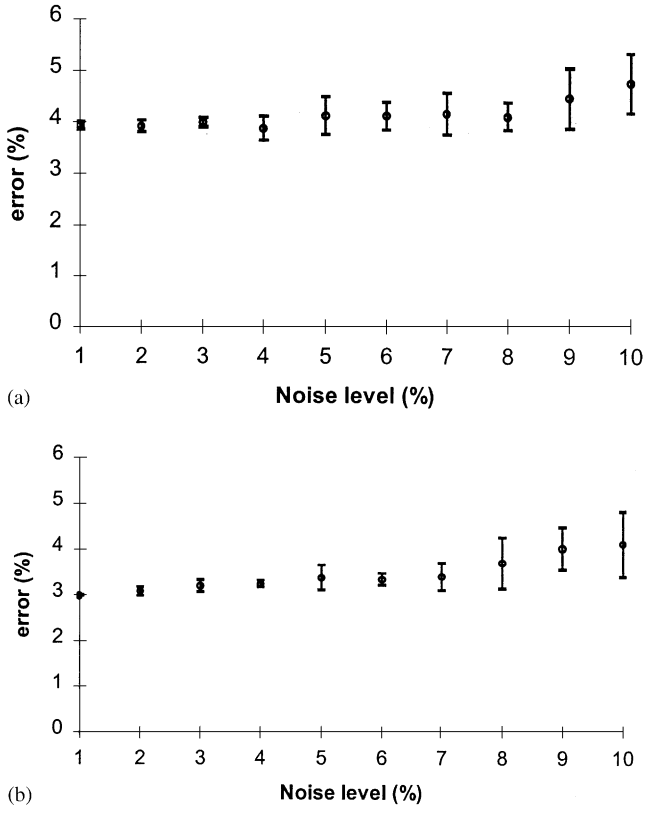


Figure 3. The mean (circles) and standard deviation (error bars) of the errors in the identified moving loads using FEM: (a) errors in the identified first moving load and (b) errors in the identified second moving load.

The errors from using FEM exhibit little change with the noise level in the responses. This is because the orthogonal function approximation in the identification reduces the effect of noise by its own filter. When the noise level in the responses increases, the standard deviation in the errors also increases. This indicates that the ESM could give very accurate results at low noise level, but it is greatly influenced by the noise effect. While the orthogonal function approximation in the FEM reduces consistently the noise effect to give accurate results in all cases studied.

### 4.3. STUDY 2: EFFECT OF MODE TRUNCATION

The first 2, 3, 4, 5 and 6 modes are used in the identification in turn. Figures 4 and 5 show the errors in the identified results with different number of modes using ESM and FEM, respectively, and Figure 6 shows the errors in the identified results with different number of terms in the orthogonal function in FEM when six modes are included in the responses.

The errors derived from ESM increase roughly proportional to the noise level in the responses and with similar gradient of change for different number of modes. The errors from using FEM exhibit little change with noise. This shows that the errors in the

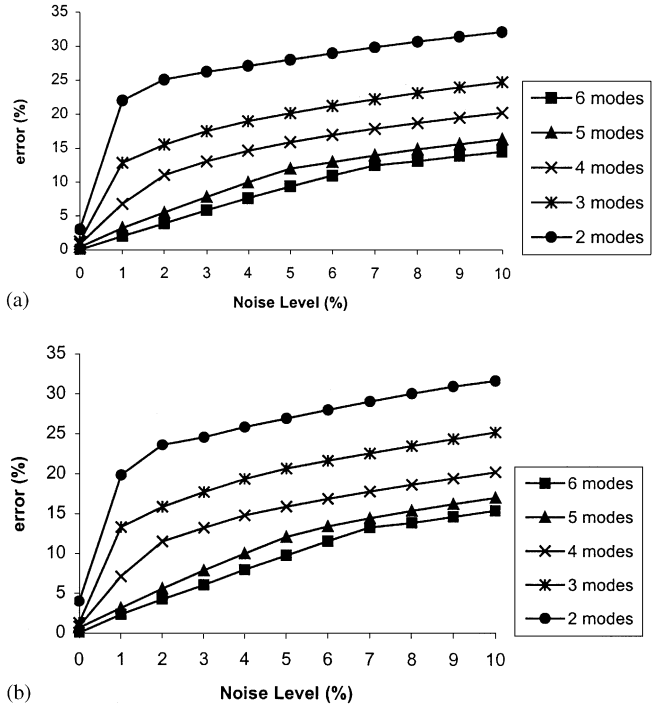


Figure 4. Errors in the identified moving loads using ESM: (a) error in the identified first moving load and (b) errors in the identified second moving load.

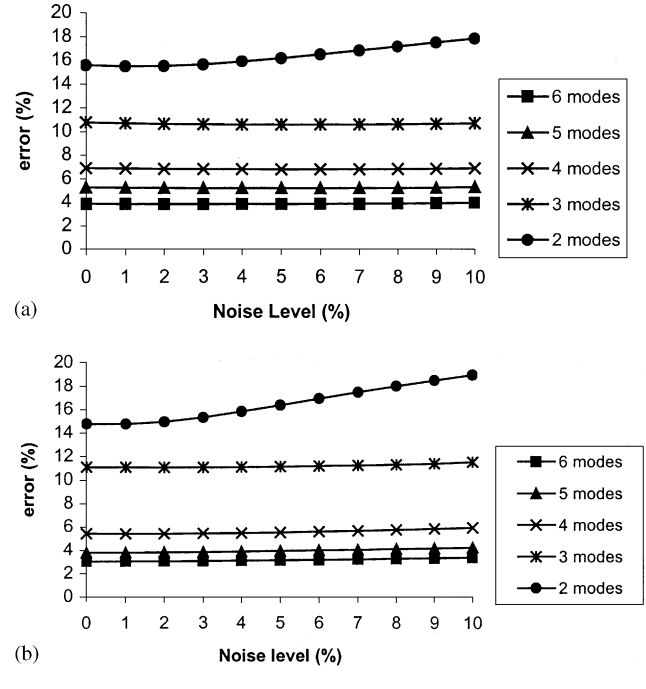


Figure 5. Errors in the identified moving loads using FEM: (a) error in the identified first moving load and (b) error in the identified second moving load.

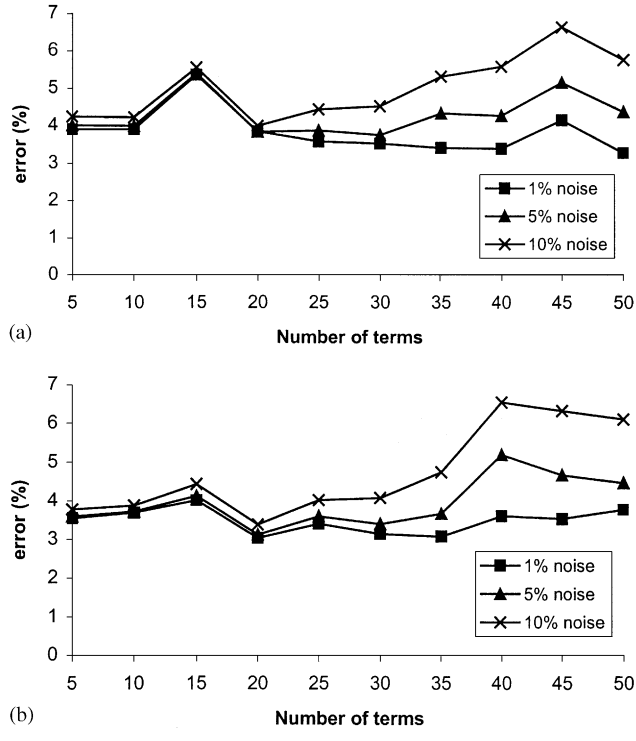


Figure 6. Errors in the identified moving loads using different number of terms in the orthogonal function: (a) error in the identified first moving load and (b) error in the identified second moving load.

identified results using FEM are mainly governed by the efficiency of the filtering effect in the orthogonal function approximation. FEM is, in general, much better than ESM in identification.

The errors shown in Figures 4 and 5 increase by a great extent when the number of modes in the identification is less than three. This is because the first three natural frequencies of the beam cover the frequency range of the moving loads, and the responses contain most of the effect from the moving loads. The errors in the identified forces in Figure 6 remain relatively constant for different noise levels when the number of terms in the orthogonal function in FEM is less than 20. And the noise level would have a negative effect on the errors when there are more terms in the orthogonal function. This is because the frequency range in the orthogonal function increases with increasing number of terms, and the high-frequency components in the noise would be retained in the calculation affecting the final results.

### 4.4. STUDY 3: EFFECT OF NUMBER OF MEASURING POINTS

The number of measuring points is selected as 6, 7, 8, 9, 10 in turn. The measuring points are evenly distributed on the beam. Figures 7 and 8 show the errors in the identified results with different number of measuring points as the noise level in the responses is increased. The number of measuring points is shown to be not related to the accuracy in

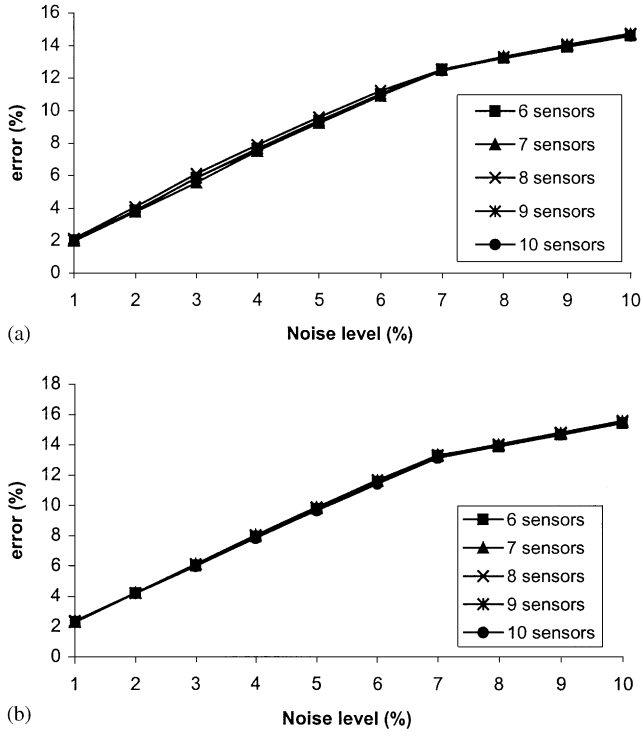


Figure 7. Errors in the identified moving loads using ESM with different number of measuring points: (a) error in the identified first moving load and (b) error in the identified second moving load.

the identified results. It should be noted that the number of measuring points used is larger than the number of the modes in the identification.

### 4.5. STUDY 4: EFFECT OF SAMPLING FREQUENCY

The responses are calculated with 0·001 s time interval between data points, and they are resampled with time intervals of 0·002 and 0·003 s in turn. Figures 9 and 10 show the errors in the identified results with different sampling frequencies and noise levels using these two methods.

The errors in the identified results for ESM are largest when the noise level is above 2% and the sampling time interval is 0·001 s. This is again due to the inclusion of more high-frequency components of noise in the calculation with a higher sampling frequency. The errors from using FEM are smaller than those from using ESM and with less variation.

### 4.6. EXAMPLE 2: SINGLE-SPAN BRIDGE SUBJECT TO A 4-D.O.F.S MOVING VEHICLE

The bridge–vehicle system shown in Figure 11 is represented by a simply supported beam subject to a moving vehicle with two axles and four degrees-of-freedom. The parameters of the system are listed as follows:

Bridge: $L = 30\,\text{m}$, $EI = 2{\cdot}5 \times 10^{10}\,\text{N m}^2$, $\rho A = 5{\cdot}0 \times 10^3\,\text{kg/m}$, $\xi = 0{\cdot}02$ for all modes.

The characteristics of the vehicle model are adopted from [20]:

$$M_v = 17\,735\,\text{kg},\ m_1 = 1500\,\text{kg},\ m_2 = 1000\,\text{kg},\ S = 4{\cdot}27\,\text{m},$$
$$a_1 = 0{\cdot}519,\ a_2 = 0{\cdot}481,\ H = 1{\cdot}80\,\text{m}, k_{s1} = 2{\cdot}47 \times 10^6\,\text{N/m},\ k_{s2} = 4{\cdot}23 \times 10^6\,\text{N/m},$$
$$k_{t1} = 3{\cdot}74 \times 10^6\,\text{N/m},\ k_{t2} = 4{\cdot}60 \times 10^6\,\text{N/m}, c_{s1} = 3{\cdot}00 \times 10^4\,\text{N/m}\,s,$$
$$c_{s2} = 4{\cdot}00 \times 10^4\,\text{N/m}\,s,\ c_{t1} = 3{\cdot}90 \times 10^3\,\text{N/m}\,s,\ c_{t2} = 4{\cdot}30 \times 10^3\,\text{N/m}\,s,$$
$$I_v = 1{\cdot}47 \times 10^5\,\text{kg}\,m^2.$$

The first six natural frequencies of the bridge deck are 3·90, 15·61, 35·13, 62·45, 97·58 and 140·51 Hz. The natural frequencies of the vehicle are 10·27, 14·44, 65·05 and 94·90 Hz. The first six bridge modes are used in the calculation of the interaction forces by the method developed by Henchi *et al.* [5]. The weight ratio between the vehicle and bridge is 0·135.

### 4.7. STUDY 5: EFFECT OF ROAD SURFACE ROUGHNESS AND MOVING SPEED

Based on ISO-8606 [21] specification, the road surface roughness in the time domain is simulated by applying the inverse fast fourier transformation [5]. Tables 1 and 2 show the errors in the identified moving loads with different moving speeds and road surface roughness using these two methods. Figure 12 shows the identified moving loads with Class *B* road surface roughness and 5% noise level in the responses.

The identified time histories are shown varying about the true time histories in Figure 12. These two methods can be used to identify the bridge–vehicle interaction forces from the bridge responses, and acceptable results can be obtained with different road surface roughness and moving speeds in the identification. The moving speed has little effect on the identified moving loads from these two methods.

In the FEM, the errors in the identified results increase as the road surface roughness increases, but they change slightly for different noise levels. This is because the high-frequency components induced by the road surface roughness are reduced by the filtering with the orthogonal function approximation. In the ESM, the errors in the identified results change slightly as the road surface condition deteriorates. However, they are also sensitive to the noise level in the responses. It may be concluded that the ESM is good for low noise level and FEM is good for high noise level in the responses.

### 4.8. STUDY 6: IDENTIFICATION OF MOVING LOADS ON BRIDGE DECK WITH VARYING SPEEDS

In practice, a vehicle moves on top of the bridge deck with varying speeds, and we shall discuss the moving load identification when the instantaneous varying speed is known in this section. The responses are calculated by the method by Zhu and Law [22]. Tables 3 and 4 show the errors in the identified results with different noise levels in the responses using these two methods. Figure 13 shows the identified moving loads when the vehicle starts braking at the entry of the bridge deck with an acceleration of $-1\,\text{m/s}^2$ and 5% noise in the responses using these two methods. Figure 14 shows the identified results when the vehicle starts braking at $1/3L$ with an acceleration of $-3\,\text{m/s}^2$ and 5% noise in the responses. The road roughness is Class *B* in both cases. The results are shown under the heading "instantaneous" in the tables.

Since the instantaneous speed of the forces is known, these two methods can be used to identify the moving loads from measured strains, and acceptable results can be obtained from both methods at low noise level. Those from using FEM are consistently much better

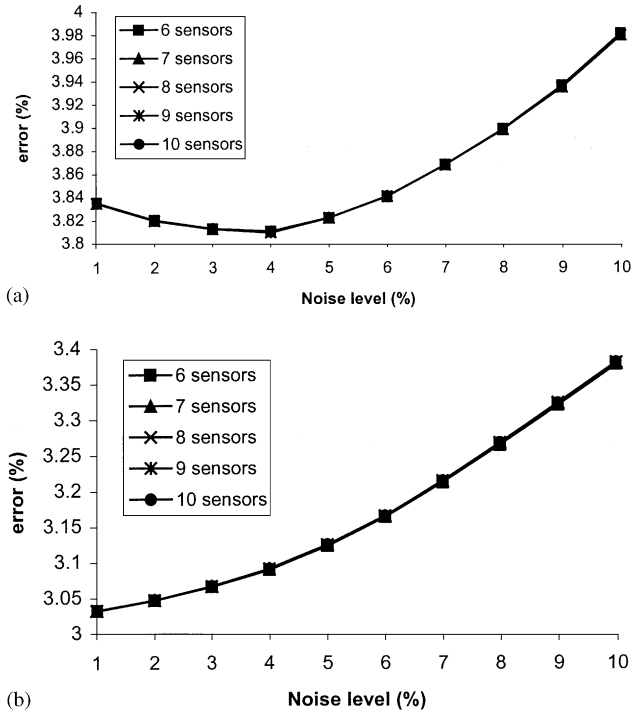


Figure 8. Errors in the identified moving loads using FEM with different number of measuring points: (a) error in the identified moving load and (b) errors in the identified second moving load.

than those from using ESM for different noise levels in the study due to its own filtering effect.

### 4.9. STUDY 7: IDENTIFICATION WITH INCOMPLETE VEHICLE SPEED INFORMATION

In practice, the axle spacing, the number of axles of the vehicle, and the time that the vehicle enters or exits the bridge can be measured directly by axle sensors. But the position of braking of vehicle and its acceleration are difficult to measure. The errors induced from identifying using an average speed should be studied. Figure 15 shows the identified results when the vehicle starts braking at the entry with an acceleration of $-1\,\mathrm{m/s^2}$ using these two methods. An average speed of 29·39 m/s is used. Figure 16 shows the identified results when the vehicle starts braking at $1/3L$ and the acceleration is $-3\,\mathrm{m/s^2}$. An average speed of 29·04 m/s is used. The road roughness is Class *B* in both cases. Tables 3 and 4 show the errors in the identified results with different noise levels in the responses. The results are shown under the heading "average" in the tables.

It is seen that the identified results from both methods using the average speed are acceptable when the acceleration is $-1\,\mathrm{m/s^2}$. But for the case with $-3\,\mathrm{m/s^2}$ acceleration, a large increase in the error for the second axle load is observed. This shows that the moving loads can be identified from strains using the average speed when the acceleration is not very large.

In the figures, the first moving load is seen overestimated and the second moving load is underestimated in both the methods. This is because the moving loads are estimated by

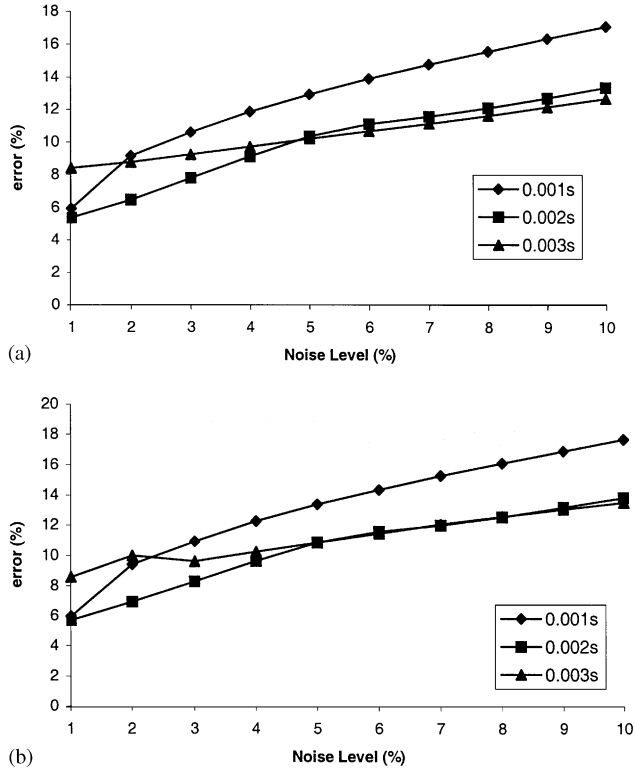


Figure 9. Errors in the identified moving loads with different sampling frequencies using ESM: (a) errors in the identified first moving load and (b) errors in the identified first moving load.

minimizing the error between the measured and reconstructed responses from the identified moving loads. The location of the resultant load using average speed lags behind that of the true resultant load and this difference is largest at mid-span of the bridge deck. The optimization, however, yields a location of the resultant load which is close and behind the true load. This leads to an overestimated first axle load and an underestimated second axle load. This behaviour is opposite in the case of having acceleration of the vehicle.

## 5. EXPERIMENTAL STUDIES

The experimental set-up is shown in Figure 17. The main beam located in the laboratory is 3678 mm long with a $100 \times 25\,\text{mm}^2$ uniform cross-section. There is a leading beam for accelerating the vehicle and a tailing beam to accept the vehicle when it comes out of the main span. The beams are simply supported and the ends of the beams are placed close together leaving only a very narrow gap of approximately 1 mm. This is necessary in order not to have a large impulsive force on the beam when the wheels cross the gap. A U-shaped aluminium section is glued to the upper surface of the beams as a direction guide for the car. The model car is pulled along the guide by a string wound around the drive wheel of an electric motor. The model car has two axles at a spacing of 0·557 m and it runs on four steel wheels with rubber band on the outside. The mass of the whole car is 16·6 kg

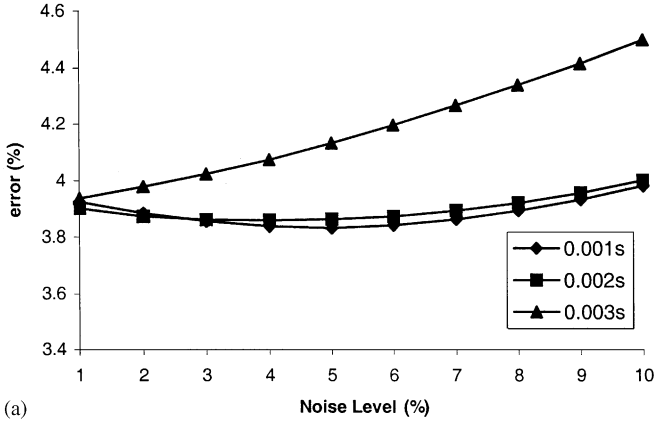


(a)

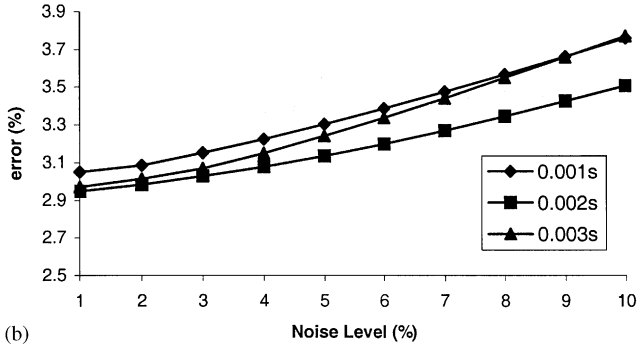


(b)

Figure 10. Errors in the identified results with different sampling frequencies using FEM: (a) errors in the first identified moving load and (b) errors in the second identified moving load.

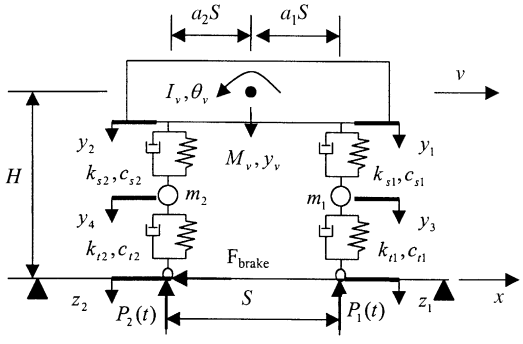


Figure 11. Bridge–vehicle system model.

with the front axle load and the rear axle load weighing 9·8 and 6·8 kg respectively. The transverse spacing between wheels is 0·08 m. Thirteen photoelectric sensors are mounted on the beams at approximately equal spacing to measure and monitor the moving speed of the car. Seven strain gauges are evenly distributed on the beam at $1/8L$. A TEAC 14-channels magnetic tape recorder and an 8-channel dynamic testing and analysis system

TABLE 1

*Errors in the identified moving loads using FEM with different moving speeds and road surface roughness (in per cent)*

| Speed (m/s) | Roughness | 1% noise | | 5% noise | | 10% noise | |
|---|---|---|---|---|---|---|---|
| | | Error 1 | Error 2 | Error 1 | Error 2 | Error 1 | Error 2 |
| | No | 2·988 | 3·909 | 3·128 | 4·067 | 3·458 | 4·444 |
| 20 | A | 3·412 | 3·416 | 3·562 | 3·530 | 3·890 | 3·844 |
| | B | 4·062 | 4·884 | 4·158 | 4·909 | 4·424 | 5·031 |
| | C | 11·312 | 15·747 | 11·316 | 15·742 | 11·391 | 15·807 |
| | D | 21·029 | 28·115 | 21·046 | 28·163 | 21·108 | 28·247 |
| 30 | No | 2·290 | 2·457 | 2·404 | 2·523 | 2·806 | 2·822 |
| | A | 3·126 | 3·108 | 3·182 | 3·181 | 3·430 | 3·446 |
| | B | 4·043 | 4·056 | 4·046 | 4·118 | 4·245 | 4·326 |
| | C | 11·691 | 13·279 | 11·654 | 13·344 | 11·676 | 13·487 |
| | D | 21·773 | 24·674 | 21·746 | 24·714 | 21·769 | 24·796 |
| 40 | No | 2·827 | 3·279 | 3·264 | 3·352 | 3·983 | 3·737 |
| | A | 3·203 | 4·104 | 3·509 | 4·054 | 4·124 | 4·207 |
| | B | 3·879 | 4·971 | 4·111 | 4·908 | 4·612 | 5·005 |
| | C | 10·714 | 13·110 | 10·770 | 13·022 | 10·932 | 13·059 |
| | D | 18·798 | 24·385 | 18·756 | 24·319 | 18·780 | 24·324 |

Error 1—error in the first axle load; Error 2—error in the second axle load.

TABLE 2

*Errors in the identified moving loads using ESM with different moving speeds and road surface roughness (in per cent)*

| Speed (m/s) | Roughness | 1% noise | | 5% noise | | 10% noise | |
|---|---|---|---|---|---|---|---|
| | | Error 1 | Error 2 | Error 1 | Error 2 | Error 1 | Error 2 |
| 20 | No | 1·997 | 2·235 | 8·631 | 9·009 | 14·206 | 14·463 |
| | A | 2·009 | 2·250 | 8·591 | 9·020 | 13·992 | 14·416 |
| | B | 2·026 | 2·269 | 8·610 | 9·072 | 13·904 | 14·434 |
| | C | 2·379 | 2·631 | 9·842 | 10·539 | 14·262 | 15·633 |
| | D | 3·199 | 3·557 | 13·263 | 14·240 | 18·527 | 19·098 |
| 30 | No | 2·091 | 2·246 | 9·238 | 9·619 | 14·435 | 14·843 |
| | A | 2·081 | 2·210 | 9·163 | 9·479 | 14·255 | 14·722 |
| | B | 2·083 | 2·193 | 9·150 | 9·419 | 14·169 | 14·696 |
| | C | 2·290 | 2·227 | 9·886 | 9·697 | 14·290 | 15·421 |
| | D | 2·858 | 2·648 | 12·247 | 11·623 | 18·523 | 17·901 |
| 40 | No | 2·008 | 2·349 | 8·843 | 9·534 | 14·623 | 15·466 |
| | A | 2·052 | 2·395 | 8·960 | 9·737 | 14·544 | 15·601 |
| | B | 2·091 | 2·435 | 9·095 | 9·919 | 14·544 | 15·752 |
| | C | 2·622 | 2·979 | 11·190 | 12·457 | 15·683 | 18·501 |
| | D | 3·372 | 4·031 | 14·336 | 17·443 | 19·652 | 22·532 |

Error 1—error in the first axle load; Error 2—error in the second axle load.

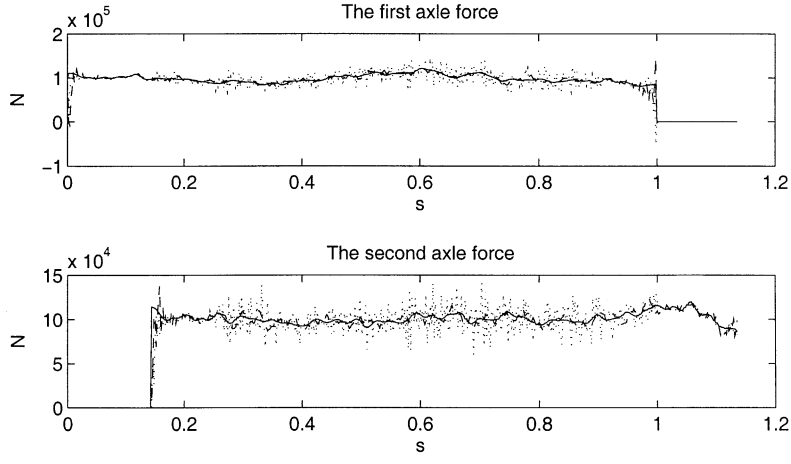


Figure 12. Identified forces on Class *B* road with 5% noise (——, true forces; – – –, using FEM; · · · · · · using ESM).

TABLE 3

*Errors (in per cent) in the moving loads identified with varying speeds using FEM*

| Noise level (%) | $-1\,m/s^2$ (braking at entry) | | | | $-3\,m/s^2$ (braking at $1/3L$) | | | |
|---|---|---|---|---|---|---|---|---|
| | Instantaneous | | Average | | Instantaneous | | Average | |
| | Error 1 | Error 2 | Error 1 | Error 2 | Error 1 | Error 2 | Error 1 | Error 2 |
| 1 | 4·129 | 5·370 | 5·081 | 7·020 | 3·555 | 5·568 | 6·986 | 14·848 |
| 2 | 4·094 | 5·307 | 5·064 | 6·968 | 3·529 | 5·568 | 6·988 | 14·822 |
| 3 | 4·065 | 5·246 | 5·049 | 6·934 | 3·520 | 5·575 | 6·993 | 14·798 |
| 4 | 4·051 | 5·203 | 5·038 | 6·985 | 3·516 | 5·588 | 7·000 | 14·776 |
| 5 | 4·045 | 5·214 | 5·029 | 7·096 | 3·518 | 5·609 | 7·005 | 14·756 |
| 6 | 4·045 | 5·348 | 5·024 | 7·213 | 3·524 | 5·634 | 7·011 | 14·736 |
| 7 | 4·049 | 5·523 | 5·031 | 7·337 | 3·535 | 5·666 | 7·019 | 14·719 |
| 8 | 4·060 | 5·705 | 5·042 | 7·468 | 3·552 | 5·703 | 7·027 | 14·704 |
| 9 | 4·076 | 5·894 | 5·055 | 7·604 | 3·574 | 5·743 | 7·037 | 14·696 |
| 10 | 4·099 | 6·086 | 5·069 | 7·743 | 3·600 | 5·787 | 7·047 | 14·696 |

Error 1—error in the first axle load; Error 2—error in the second axle load.

are used for data collection and analysis in the experiment. The sampling frequency is 2000 Hz. The recorded length of each test sample lasts for 6 s. Braking force is applied with a set of rubber bands placed transversely in front of the vehicle approximately at the level of its centroid, and the braking force was tuned by adjusting the tension in the rubber band.

The first three natural frequencies of the model car are 7·82, 9·77 and 11·72 Hz and those of the main beam are 3·67, 16·83 and 37·83 Hz. The car was placed at the right end of the leading beam, and the data acquisition system was set in the pre-trigger state. The power for the motor was then turned on, and the car moved on the top of the beam. The vibration signals were recorded. The zeroshift in the measured signals was removed, and the signals were calibrated with their measured sensitivities. The point in the signals when the front wheel of the car just got on the main beam was identified.

TABLE 4

*Errors (in per cent) in the moving loads identified with varying speeds using ESM*

| Noise level (%) | $-1\,m/s^2$ (braking at entry) | | | | $-3\,m/s^2$ (braking at $1/3L$) | | | |
|---|---|---|---|---|---|---|---|---|
| | Instantaneous | | Average | | Instantaneous | | Average | |
| | Error 1 | Error 2 | Error 1 | Error 2 | Error 1 | Error 2 | Error 1 | Error 2 |
| 1 | 1·930 | 2·630 | 4·907 | 6·895 | 1·874 | 2·739 | 8·026 | 15·682 |
| 2 | 3·644 | 4·655 | 5·659 | 7·825 | 3·504 | 5·088 | 8·265 | 15·921 |
| 3 | 5·297 | 6·674 | 6·730 | 9·158 | 5·099 | 7·395 | 8·734 | 16·467 |
| 4 | 6·968 | 8·663 | 7·955 | 10·689 | 6·664 | 6·655 | 9·396 | 17·296 |
| 5 | 8·622 | 10·647 | 9·322 | 12·309 | 8·205 | 11·873 | 10·086 | 18·368 |
| 6 | 10·825 | 12·583 | 10·715 | 14·004 | 9·712 | 14·056 | 10·305 | 19·790 |
| 7 | 11·825 | 14·440 | 11·137 | 14·773 | 11·160 | 16·191 | 10·553 | 20·955 |
| 8 | 12·291 | 13·724 | 11·778 | 15·660 | 11·759 | 15·042 | 10·988 | 21·916 |
| 9 | 13·109 | 14·497 | 12·390 | 16·516 | 12·568 | 15·889 | 11·440 | 22·764 |
| 10 | 13·858 | 15·244 | 12·989 | 17·321 | 13·330 | 16·690 | 11·899 | 23·540 |

Error 1—error in the first axle load; Error 2—error in the second axle load.

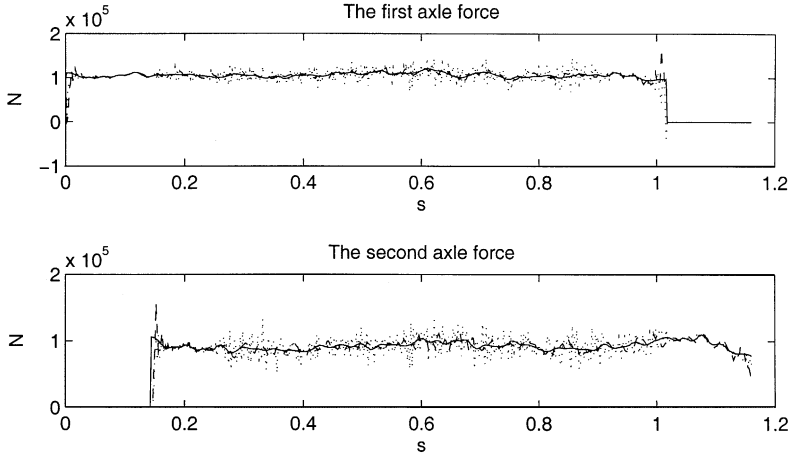


Figure 13. Identified forces on instantaneous speed and braking at entry (——, true forces; – – –, using FEM; · · · · · · using ESM).

## 5.1. IDENTIFICATION WITH CAR TRAVELLING AT UNIFORM SPEED

The first experiment is conducted with the vehicle moving approximately at 1·25 m/s, and the strains collected are resampled at 200 Hz to include the first three vibration modes. Figure 18 shows the identified results from strains at $1/4L$, $1/2L$ and $3/4L$ with the first three modes using both methods.

The mean values of the identified loads are close to and varying around the static loads using these two methods. Results from using FEM are in general worse than those from using ESM. This is because the noise level in the measurement is low, and the error of identification from ESM is smaller than that from FEM when the number of vibration mode used is small as observed from the simulation results in Figures 4 and 5.

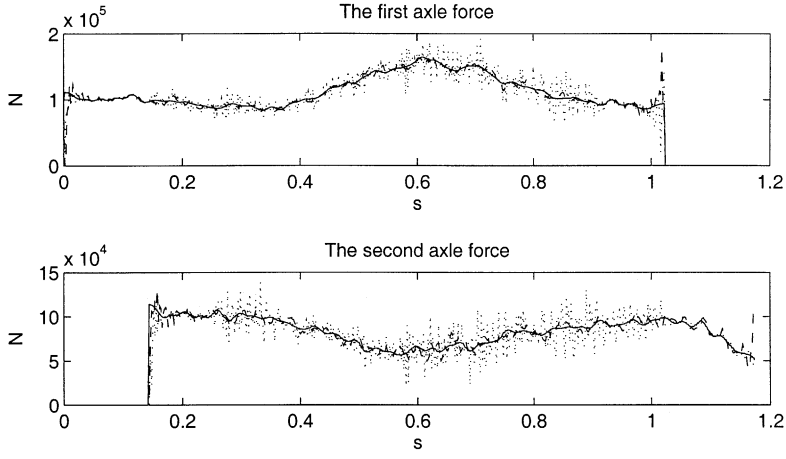


Figure 14. Identified forces on instantaneous speed and braking at $1/3L$ (——, true forces; – – –, using FEM; · · · · · · using ESM).

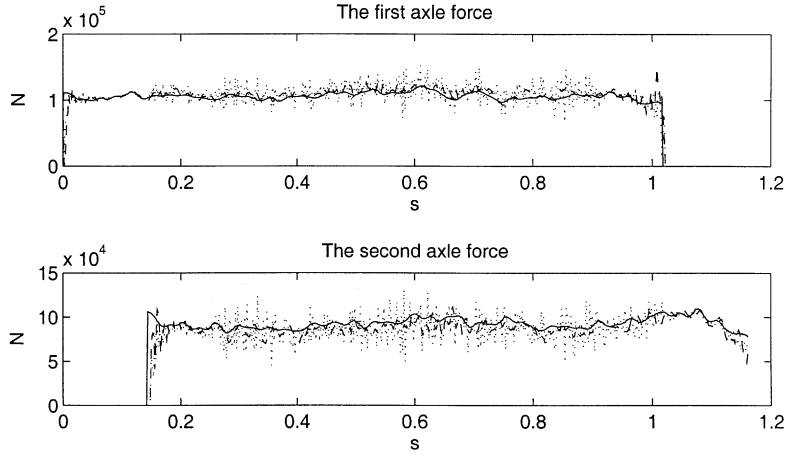


Figure 15. Identified forces using average speed with braking at entry (——, true forces; – – –, using FEM; · · · · · · using ESM).

## 5.2. IDENTIFICATION WITH BRAKING STARTS AT 0·878 m

The parameters are the same as for the above experiment. The moving car starts braking at 0·878 m. The actual speed measured between adjacent pairs of photoelectric sensors is shown in Table 5 with an average of 1·19 m/s. The moving car accelerates before braking and it crosses the beam completely with deceleration. Figure 19 shows the identified loads from strains at $1/4L$, $1/2L$ and $3/4L$ for the car moving at the true and the average speed using ESM. The reconstructed strains at $5/8L$ are also compared with the measured strain. The correlation coefficients between them are, respectively, 0·983 and 0·985, and the optimal regularization parameters are, respectively, $8{\cdot}040 \times 10^{-16}$ and $8{\cdot}267 \times 10^{-16}$ for the cases identified using true and average speeds. Figure 20 shows the identified results from FEM using the same set of strains for the car moving at the true and average speed.

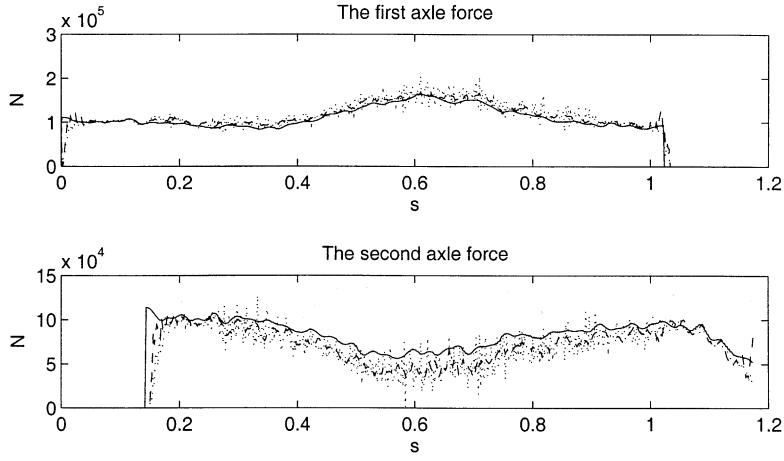


Figure 16. Identified forces using average speed with braking at $1/3L$ (——, true forces; – – –, using FEM; · · · · · · using ESM).

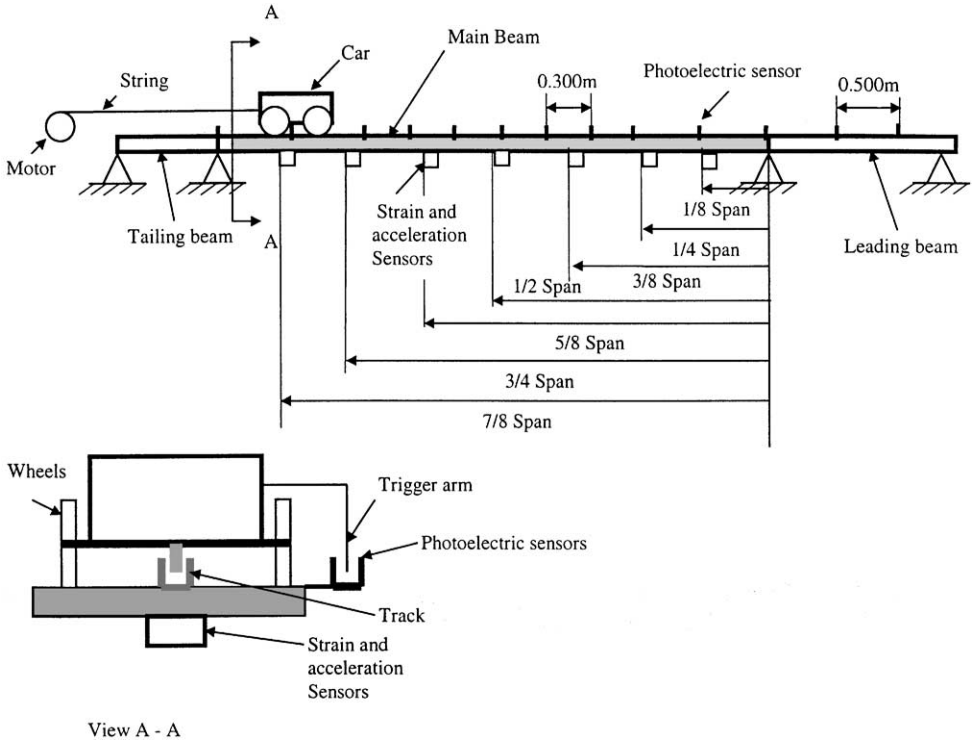


Figure 17. Diagrammatic drawing of the experimental set-up.

Large fluctuations are found in the identified loads in Figures 19 and 20. This is due to the pitching motion induced by the horizontal braking force. Impulsive interaction forces generated from braking would also cause these fluctuations. The identified loads differ slightly when the true or average speed is used. The second axle load identified from using

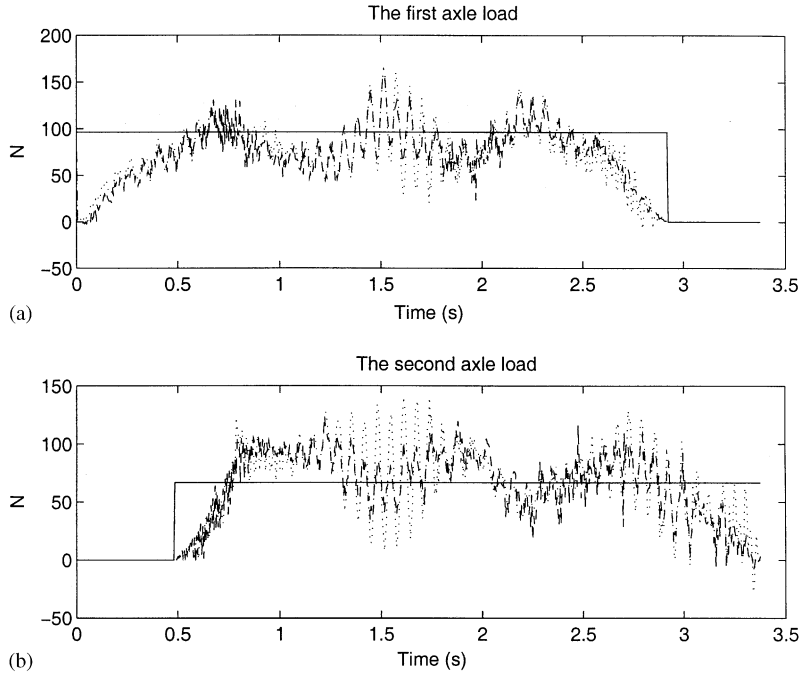


Figure 18. Identification from strains at $1/4L$, $1/2L$, $3/4L$ (——, static forces; – – –, using ESM; · · · · · · using FEM).

TABLE 5

*Transient speed in experiment*

| Range of distance (m) | 0·0–0·478 | 0·478–0·878 | 0·878–1·178 | 1·178–1·478 | 1·478–1·778 | 1·778–2·078 | 2·078–2·378 | 2·378–2·678 | 2·678–3·178 | 3·178–3·678 |
|---|---|---|---|---|---|---|---|---|---|---|
| Velocity (m/s) | 1·215 | 1·305 | 1·271 | 1·250 | 1·245 | 1·139 | 1·154 | 1·149 | 1·129 | 1·119 |

average speed is underestimated and the first axle load is overestimated from both methods. This observation is similar to those found in the simulation studies and is due to the acceleration of the car. There is very small difference in the curves close to the ends of the beam because the difference of the location of the resultant forces calculated from the average speed and the instantaneous speed is very small.

## 6. CONCLUSIONS

Both the FEM and the ESM can be used to identify the moving loads or the bridge–vehicle interaction forces from measured strains with road roughness and vehicle braking on the bridge. The FEM gives consistently smaller error in the results for all noise levels, while the accuracy of ESM is greatly affected by noise. This indicates the importance of having pre-processing of the measured data to remove the measurement noise before the

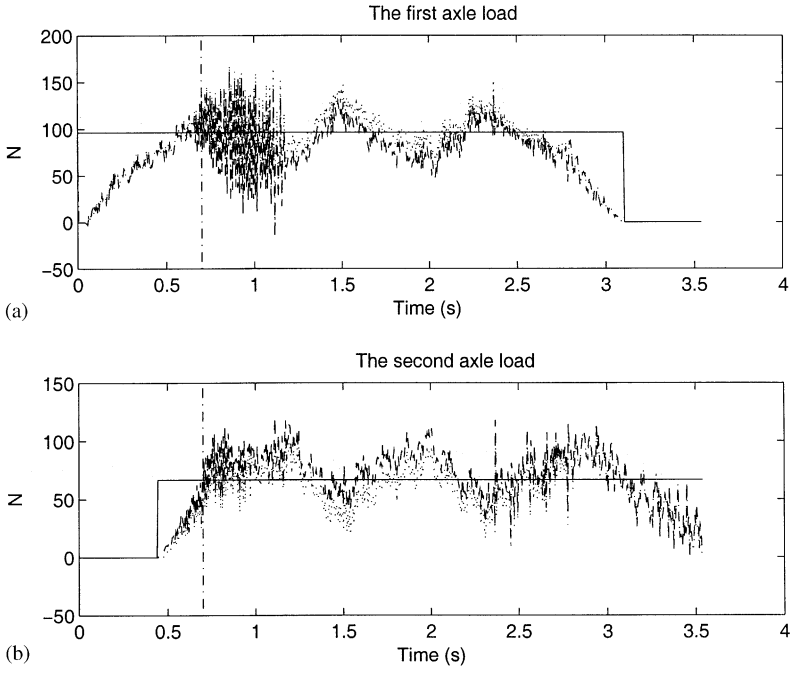


Figure 19. Identification from strains using ESM when braking starts at 0·878 m (——, static loads; – – –, results using varying speed; · · · · · ·, results using average speed; –·–·, start braking position).

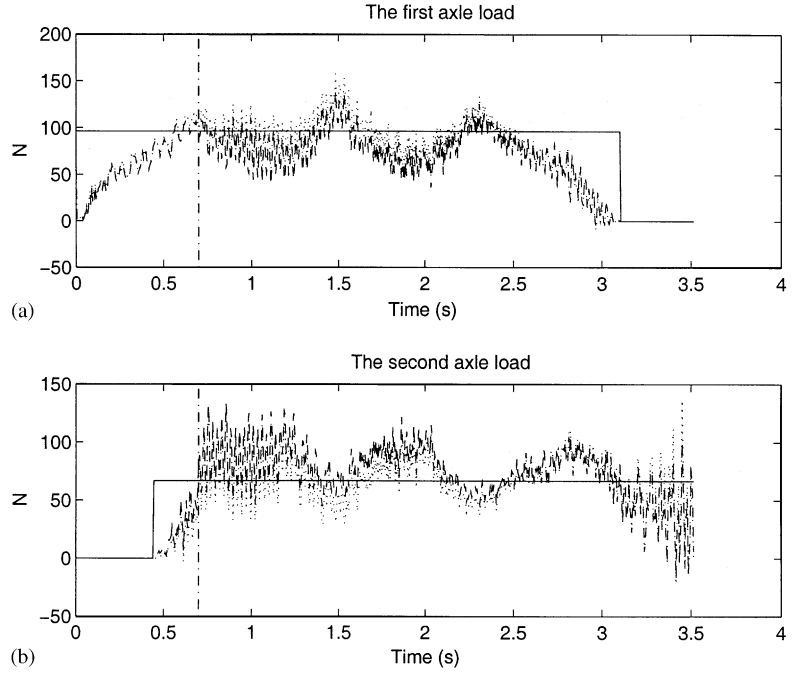


Figure 20. Identification from strains using FEM when braking starts at 0·878 m (——, static loads; – – –, results using varying speed; · · · · · ·, results using average speed; –·–·, start braking position).

identification. The orthogonal function approximation of the measured strains is also shown to be effective in filtering the high-frequency noise components in the responses.

From the parametric studies conducted, the speed of forces and the number of sensors have no effect on the accuracy of results. The sampling frequency, the number of measuring points and the number of modes included in the identification are conditional to the accuracy. The sampling frequency should be higher than the frequency range in the responses while the number of modes should cover the frequency range of the forces to be identified. The number of measuring points should be larger than the number of modes used in the identification. The road surface roughness Classes *A, B* and *C* have little effect on the accuracy while Class *C* and *D* would cause large error in the identified results from both methods. A small acceleration of $-1\,\mathrm{m/s^2}$ on an average of $30\,\mathrm{m/s^2}$ does not have large effect on the accuracy of identification, but a large acceleration of $-3\,\mathrm{m/s^2}$ would cause large error in the second axle force. And the first axle load is overestimated while the second axle load is underestimated with identification of decelerating forces using an average speed and *vice versa*.

## ACKNOWLEDGMENTS

The work described in this paper was supported by a grant from the Hong Kong Polytechnic University Research Funding Project No. V653.

## REFERENCES

1. R. Cantineni 1992 *Swiss Federal Laboratories for Materials Testing and Research* (EMPA) Report No. 220, 240pp. Dynamic behavior of highway bridges under the passage of heavy vehicles.
2. R. J. Heywood 1994 *International Journal of Vehicle Design*. Influence of truck suspensions on the dynamic response of a short span bridge.
3. M. F. Green and D. Cebon 1997 *Computers and Structures* **62**, 253–264. Dynamic interaction between heavy vehicle and highway bridges.
4. Y. B. Yang and J. D. Yau 1997 *Journal of Structural Engineering American Society of Civil Engineers* **123**, 1512–1518. Vehicle-bridge interaction element for dynamic analysis.
5. K. Henchi, M. Fafard, M. Talbot and G. Dhatt 1998 *Journal of Sound and Vibration* **212**, 663–683. An efficient algorithm for dynamic analysis of bridges under moving vehicles using a coupled modal and physical components approach.
6. R. J. Peters 1984 *Proceedings of the* 12*th ARRB Conference* **12**, 10–18. A system to obtain vehicle axle weights.
7. T. J. Peters 1986 *Proceedings of the* 13*th ARRB and 5th REAAA Combined Conference* Part 6, 70–83. An unmanned and undetectable highway speed vehicle weighing system.
8. S. S. Law, T. H. T. Chan and Q. H. Zeng 1997 *Journal of Sound and Vibration* **201**, 1–22. Moving force identification: time domain method.
9. S. S. Law, T. H. T. Chan and Q. H. Zeng 1999 *Journal of Dynamic Systems, Measurement and Control American Society of Mechanical Engineers* **121**, 394–401. Moving force identification: a frequency-time domain method.
10. S. S. Law, T. H. T. Chan, X. Q. Zhu and Q. H. Zeng 2001 *Journal of Engineering Mechanics American Society of Civil Engineers* **127**, 136–148. Regularization in moving force identification.
11. X. Q. Zhu and S. S. Law 2000 *Journal of Sound and Vibration* **236**, 705–724. Identification of vehicular axle loads from bridge dynamic responses.
12. C. O'Connor and T. H. T. Chan 1988 *Journal of Structural Engineering American Society of Civil Engineers* **114**, 1703–1723. Dynamic wheel loads from bridge strains.
13. T. H. T. Chan, S. S. Law, T. H. Yung and X. R. Yuan 1999 *Journal of Sound and Vibration* **219**, 503–524. An interpretive method for moving force identification.
14. S. S. Law and Y. L. Fang 2001 *Journal of Sound and Vibration* **239**, 233–254. Moving force identification: Optimal state estimation approach.

15. T. H. T. Chan, Ling Yu and S. S. Law 2000 *Journal of Sound and Vibration* **235**, 87–104. Comparative studies on moving force identification from bridge strains in laboratory.
16. X. Q. Zhu and S. S. Law 2001a *Journal Sound and Vibration* **245**, 329–345. Orthogonal function in moving loads identification on a multi-span bridge.
17. T. Hayashikawa and N. Watanabe 1981 *Journal of the Engineering Mechanics Division American Society of Civil Engineers* **107**, 229–246. Dynamic behavior of continuous beams with moving loads.
18. G. H. Golub, M. Heath and G. Wahba 1979. *Technometrics* **21**, 215–223. Generalized cross-validation as a method for choosing a good ridge parameter.
19. P. C. Hansen 1992. *SIAM Review* **34**, 561–580. Analysis of discrete ill-posed problems by means of the L-curve.
20. N. L. Mulcahy 1983 *Earthquake Engineering and Structural Dynamics* **11**, 649–665. Bridge response with tractor-trailer vehicle loading.
21. ISO8606: 1995(E) *International Standards Organization*. Mechanical vibration—road surface profiles—reporting of measured data.
22. X. Q. Zhu and S. S. Law 2001b *Journal of Sound and Vibration* **240**, 962–970. Precise time step integration for the dynamic response of a continuous beam under moving loads.

## APPENDIX A: NOTATION

| | |
|---|---|
| $\rho$ | mass per unit length of beam |
| $A$ | cross-sectional area |
| $E$ | Young's modulus of material |
| $I$ | second moment of inertia |
| $L$ | total length of beam |
| $N$ | number of modes or number of degree-of-freedom of a system |
| $N_s$ | number of measuring points |
| $N_t$ | number of data points |
| $N_p$ | number of moving loads |
| $M_i$ | modal mass of the $n$th mode |
| $M_v, I_v$ | mass and inertia moment of the vehicle |
| $P_l(t)$ | time varying concentrated load |
| $S$ | axle spacing |
| $\mathbf{B}$ | coefficient matrix |
| $\mathbf{P}$ | load vector |
| $a_1, a_2$ | position parameters |
| $c$ | viscous damping of beam |
| $h_i(t)$ | impulse response |
| $k_{si}, c_{si}$ | stiffness and damping of the suspension system |
| $k_{ti}, c_{ti}$ | stiffness and damping of the tyres |
| $m_1, m_2$ | mass of two tyres |
| $q_i(t)$ | $n$th modal co-ordinate |
| $v(t)$ | travelling velocity of force |
| $w(x, t)$ | displacement function of beam |
| $x_s$ | location of the measuring point |
| $z_t$ | distance between the bottom surface and the neutral surface of beam |
| $\hat{x}_l(t)$ | location of moving load $P_l(t)$ at time $t$ |
| $\delta(t)$ | the Dirac delta function |
| $\phi_i(x)$ | mode shape of $n$th mode |
| $\lambda$ | regularization parameter |
| $\xi_i, \omega_i$ | damping ratio and frequency of $i$th mode respectively |
| $\omega_i'$ | damped $i$th modal frequency |
| $\varepsilon(x, t)$ | strain at location $x$ and time $t$ |
| $\boldsymbol{\varepsilon}, \ddot{\mathbf{w}}$ | vector of strain |